The TRMM Multi-satellite Precipitation Analysis (TMPA)

George J. Huffman[1,2], Robert F. Adler[1,3], David T. Bolvin[1,2], Eric J. Nelkin[1,2]

1: NASA/GSFC Laboratory for Atmospheres
2: Science Systems and Applications, Inc.
3: Earth System Science Interdisciplinary Center,
   Univ. of Maryland College Park

Corresponding author:

George J. Huffman
NASA/GSFC Code 613.1
Greenbelt, MD 20771

Phone: 301-614-6308
Fax: 301-614-5492
Email: george.j.huffman@nasa.gov

Abstract

The Tropical Rainfall Measuring Mission (TRMM) Multi-satellite Precipitation Analysis (TMPA) is intended to provide a "best" estimate of quasi-global precipitation from the wide variety of modern satellite-borne precipitation-related sensors. Estimates are provided at relatively fine scales (0.25°x0.25°, 3-hourly) in both real and post-real time to accommodate a wide range of researchers. However, the errors inherent in the finest scale estimates are large. The most successful use of the TMPA data is when the analysis takes advantage of the fine-scale data to create time/space averages appropriate to the user's application. We review the conceptual basis for the TMPA, summarize the processing sequence, and focus on two new activities. First, a recent upgrade to the real-time version incorporates several additional satellite data sources and employs monthly climatological adjustments to approximate the bias characteristics of the research quality post-real-time product. Second, an upgrade of the research quality post-real-time TMPA from Version 6 to Version 7 (in beta test at press time) is designed to provide a variety of improvements that increase the list of input data sets and correct several issues. Future enhancements for the TMPA will include improved error estimation, extension to higher latitudes, and a shift to a Lagrangian time interpolation scheme.

Keywords: precipitation, satellite, remote sensing, TRMM, GPM

1. Introduction

As elaborated elsewhere in this book, precipitation is a critical weather element for determining the habitability of different parts of the Earth, yet is difficult to measure adequately with surface-based instruments due to its small-scale variability in space and time. Thus, satellite-borne sensors play a key role in estimating precipitation. The proliferation of precipitation-sensing satellites in the last 20 years (Fig. 1) has tremendously enhanced our ability to estimate precipitation over much of the globe, but the critical piece of the puzzle is deciding how to combine all of these individual estimates to form a single, best estimate. The desired result is a stable, long, quasi-global time series of precipitation estimates on a uniform time/space grid that has the finest scale that the data will reasonably support. Several factors work against these attributes. Starting at the finest granularity, each sensor, and associated algorithms, has strengths and weaknesses that can affect its accuracy, usually varying by region. A second factor is that the constellation of precipitation-sensing satellites is uncoordinated, although operational agencies typically strive to maintain one or two specific satellites in preferred orbits. This dependence on satellites of opportunity introduces larger gaps in temporal sampling than would be the case for a coordinated constellation. As well, many of the satellites drift (Fig. 1), giving interannual changes in the gaps, even for the same complement of satellites. Finally, the number and types of satellites change over time, implying that the input data cannot be considered homogeneous. Accordingly, schemes that seek to combine all of these inputs into a "best" dataset must be designed around, and examined for, these issues.

The Tropical Rainfall Measuring Mission (TRMM) Multi-satellite Precipitation Analysis (TMPA) was designed with a heritage that includes the Adjusted Geosynchronous Operational Environmental Satellite (GOES) Precipitation Index (AGPI; Adler et al. 1994), the Global Precipitation Climatology Project (GPCP) monthly satellite-gauge (SG) combination (Huffman et al. 1997; Adler et al. 2003), and the GPCP One-Degree Daily (Huffman et al. 2001) combination estimates of precipitation. In common with these predecessor data sets, we identify a specific

a specific high-quality data set as the calibrator, and then work to make the remaining input data as consistent as possible with the calibrator data. In contrast to the earlier data sets, the TMPA is designed to use "all" available data, meaning that we are accepting the potential inhomogeneities of a time-varying complement of inputs in return for potentially better combination results when more high-quality data are available. Another difference with the earlier data sets is that the TMPA is generated twice, first as a real-time (RT) product computed about 6-9 hours after observation time, and then as a post-real-time research product computed about 15 days after the end of the month with additional data, including monthly surface rain gauge data.

The spatial resolution was chosen as 0.25°x0.25° latitude/longitude to ensure that the grid box is somewhat larger than the typical footprint size for passive microwave (hereafter "microwave") precipitation estimates, which are the coarsest estimates in common use. The spatial domain was set to 50°N-50°S because all of the microwave and infrared (IR) estimates we are using tend to lose skill at higher latitudes. The temporal resolution was chosen as three hours because 1) it allows us to resolve the diurnal cycle, 2) it matches the mandated interval for full-disk images from the international constellation of geosynchronous (geo) satellites, and 3) it provides a reasonable compromise between spatial coverage and temporal frequency for gridding the asynoptic microwave estimates from low-Earth-orbit (leo) satellites. The time spans covered by the TMPA data sets are currently determined by the start of TRMM for the research product and the start of processing for the RT product, respectively.

The following sections briefly address the instruments and input datasets that are used in the TMPA (Section 2), the methodology used to combine them (Section 3), and their current status (Section 4). Then we display some comparisons and examples (Section 5) and end by discussing future plans (Section 6).

2. Instruments and Input Datasets

The TMPA depends on input from two different types of satellite sensors, namely microwave and IR. First, precipitation-related microwave data are being collected by a variety of leo satellites (Fig. 1), including the TRMM Microwave Imager (TMI) on TRMM, Special Sensor Microwave/Imager (SSM/I) and Special Sensor Microwave Imager/Sounder (SSMIS) on Defense Meteorological Satellite Program (DMSP) satellites, Advanced Microwave Scanning Radiometer for the Earth Observing System (AMSR-E) on Aqua, the Advanced Microwave Sounding Unit B (AMSU-B) on the National Oceanic and Atmospheric Administration (NOAA) satellite series, and the Microwave Humidity Sounders (MHS) on later NOAA-series satellites and the European Operational Meteorological (MetOp) satellite. All of these data have a direct physical connection to the hydrometeor profiles above the surface, but each individual satellite provides a very sparse sampling of the time-space occurrence of precipitation. Even when composited into 3-hour datasets, the current "full" microwave coverage averages about 80% of the Earth's surface in the latitude band 50°N-S and amounted to about 40% at the beginning of the TMPA record in 1998 with three satellites. Not all of the data shown in Fig. 1 can be used in the TMPA. For example, a signal contamination problem on the F15 DMSP that began in August 2006 suspended its use, while various new sensors have not yet been incorporated into the products, including the SSMIS (DMSP F16 and F17) and MHS (NOAA 18, except in the new real-time, and MetOp).

Each microwave pixel-level observation from TMI, AMSR-E, and SSM/I is converted to a precipitation estimate with sensor-specific versions of the Goddard Profiling Algorithm (GPROF; Kummerow et al. 1996, Olson et al. 1999) for subsequent use in the TMPA. This takes place at

takes place at the Precipitation Measurement Missions' (PMM) Precipitation Processing System (PPS), formerly known as the TRMM Science Data and Information System (TSDIS). GPROF is a physically-based algorithm that applies a Bayesian least-squares fit scheme to reconstruct the observed radiances for each pixel by selecting the "best" combination of thousands of numerical-model-generated microwave channel upwelling radiances. As part of the processing the microwave data are screened for contamination by surface effects.

Microwave pixel-level from AMSU-B are converted to precipitation estimates at the National Environmental Satellite Data and Information Service (NESDIS) using operational versions of the Zhao and Weng (2002) and Weng et al. (2003) algorithm. Ice Water Path (IWP) is computed from the 89- and 150-Ghz channels, with a surface screening that employs ancillary data. Precipitation rate is then computed based on the IWP and precipitation rate relations derived from cloud model data based on the NCAR/PSU Mesoscale Model Version 5 (MM5).

The AMSU-B algorithm detects solid hydrometeors, but not liquid. The multi-channel conical-scan passive microwave sensors (TMI, AMSR, SSM/I) similarly sense only solid hydrometeors over land, so the AMSU-B estimates are roughly comparable for land areas. However, over ocean the conical scanners also sense liquid hydrometeors, providing additional sensitivity, including to precipitation from clouds that lack the ice phase. As a result, the AMSU-B estimates over ocean are relatively less capable in detecting precipitation over ocean. [Despite the over-land focus of this book, some background on "coast" and "ocean" will be given for completeness.]

The second major data source for the TMPA is the geo-IR data, which provide excellent time-space coverage, in contrast to the microwave data. However, all IR-based precipitation estimates share the limitation that the IR brightness temperatures (T_b) primarily represent cloud-top temperature, and implicitly cloud height. Arkin and Meisner (1987) showed that IR estimates are poorly correlated to precipitation at fine time/space scales, but relatively well-correlated at scales larger than about 1 day and 2.5°x2.5° of lat./long. The Climate Prediction Center (CPC) of the National Weather Service/NOAA merges geo-IR data from the five main international geo satellites into half-hourly 4x4-km-equivalent lat./long. grids for the domain 60°N-60°S (hereafter the "CPC merged IR"; Janowiak et al. 2001). This dataset contains IR T_b's corrected for zenith-angle viewing effects and inter-satellite calibration differences. At present, the research TMPA estimates generated prior to the start of the CPC merged IR data set in early 2000 are computed using a GPCP data set (also produced at CPC) that contains 24-class histograms of geo-IR T_b data on a 3-hourly, 1°x1° lat./long. grid covering the latitude band 40°N-S (hereafter the "GPCP IR histograms"; Huffman et al. 2001). This data set also includes GOES Precipitation Index (GPI; Arkin and Meisner 1987) estimates computed from leo-IR data recorded by the NOAA satellite series, averaged to the 1°x1° grid. The TMPA fills gaps in the geo-IR coverage with these data, most notably before June 1998 in the Indian Ocean sector.

Finally, the research TMPA employs three additional data sources: the TRMM Combined Instrument (TCI) estimate, which combines data from both TMI and the TRMM Precipitation Radar (PR; TRMM product 2B31; Haddad et al. 1997a,b); the Global Precipitation Climatology Centre (GPCC) monthly rain gauge analysis (Rudolf 1993); and the Climate Assessment and Monitoring System (CAMS) monthly rain gauge analysis developed by CPC (Xie and Arkin 1996).

3. General Methodology

The research-quality TMPA is computed in four stages; (1) the microwave precipitation estimates are inter-calibrated and combined, (2) IR precipitation estimates are created using the calibrated microwave precipitation, (3) the microwave and IR estimates are combined, and (4) rain gauge data are integrated. The real-time TMPA lacks the fourth step and has a few simplifications, as outlined in Section 3.3. Each TMPA precipitation field is expressed as the precipitation rate effective at the nominal observation time because most gridboxes contain data from one snapshot of satellite data.

3.1   Combined microwave estimates

Each microwave precipitation data set is averaged to the 0.25° spatial grid over the time range ±90 minutes from the nominal 3-hourly observation times (00Z, 03Z, …, 21Z). Probability matching to a "best" estimate using coincident matchups is used to adjust each sensor, similar to Miller (1972) and Krajewski and Smith (1991). Although we wish to adopt the TCI as the calibrating data source, the coincidence of TCI with any of the sensors other than TMI is sparse, so we establish a TCI–TMI calibration, then apply that to TMI. The remaining sensor data are all calibrated to TMI, and then adjusted to the TCI using the TCI-TMI calibration. The TCI–TMI relationship is computed on a 1°x1° grid for each month with the coincident data aggregated on overlapping 3°x3° windows. The TCI-TMI calibration interval for the research product is a calendar month, and the resulting adjustments are applied to data for the same calendar month. This choice is intended to keep the dependent and independent data sets for the calibrations as close as possible in time.

Preliminary work showed that the TMI calibrations of the other sensors' estimates are adequately represented by climatologically-based coefficients representing large areas. In the case of the TMI–SSM/I calibration, separate calibrations are used for five oceanic latitude bands (40-30°N, 30-10°N, 10°N-10°S, 10-30°S, 30-40°S) and a single land-area calibration for each of four three-month seasons. The TMI–AMSR-E and TMI–AMSU-B calibrations are given one climatological adjustment for land and another for ocean. The AMSU-B calibration has two additional issues. First, the NESDIS algorithm changed on 31 July 2003 and 31 May 2007, so separate sets of calibrations are provided for the data periods. Second, in all periods the AMSU-B fractional occurrence of precipitation in the subtropical highs is notably deficient. After extensive preliminary testing, the authors judged it best to develop the ocean calibration as a single region, recognizing that the resulting fields would have a somewhat low bias. Huffman et al. (2007) show that the low bias is somewhat larger than expected, but this does not affect the over-land hydrology applications on which this book focuses. In all cases the calibrations in the 40°-50° latitude belts in both hemispheres are simply taken to be the calibrations that apply just Equator-ward of 40°.

Once the microwave estimates are calibrated for each satellite and quality-controlled, the grid is filled using the "best" available data to produce the High Quality (HQ) microwave combination. The TCI alone is used, if available. Otherwise, if there are one or more overpasses from TCI-adjusted TMI, TCI-adjusted AMSR-E, and TCI-adjusted SSM/I in the 3-hr window for a given grid box, all of these data are used (averaging as necessary). The histogram of precipitation rate is somewhat sensitive to the number of overpasses averaged together, so it would be more consistent to take the single "best" overpass in the data window period. The TCI-adjusted AMSU-B estimates are only used if none of the other microwave estimates are available for the grid box, due to the detectability deficiency in the AMSU-B estimates over ocean discussed above. Detectability is equally problematic over land for AMSU-B and conical-scan sensors, so this rule is unnecessarily restrictive, but likely not a serious problem.

3.2   Microwave-calibrated IR estimates

The IR data are not provided at the 0.25° resolution, so some pre-processing is required. In the early period of the research product (1 January 1998 to 7 February 2000), each grid box's histogram in the 1°x1° 3-hourly GPCP IR histogram dataset is zenith-angle corrected, averaged to a single T_b value for the grid box, and plane-fit interpolated to the 0.25° grid. For the period from 7 February 2000 onwards, the CPC Merged IR is averaged to 0.25° resolution and combined into hourly files as ±30 minutes from the nominal time. Time-space matched HQ precipitation rates and IR T_b's are accumulated for a month into histograms of 3-hourly 0.25°x0.25° values on a 1°x1° grid, aggregated to overlapping 3°x3° windows, and then used to convert IR T_b's to precipitation rates. As in the TCI-TMI calibration for the HQ, the calibration period is the calendar month. Quality control is again applied to the HQ here to control artifacts.

The IR precipitation estimate is a simple "colder clouds precipitate more" approach, with the coldest 0.25°x0.25°-average T_b assigned the greatest observed HQ precipitation rate, and so on, with zero precipitation assigned for all T_b's warmer than a spatially varying threshold value determined by the fractional coverage of precipitation in the microwave data. Calibration coefficients in grid boxes that lack coincident data throughout the month, usually due to cold-land dropouts or quality control, are computed using smooth-filled histograms of coincident data from surrounding grid boxes. Strict probability matching tends to show unphysical fluctuations at the highest precipitation rates, so we somewhat subjectively choose to replace the coldest 0.17% of the T_b histogram by a fourth-order polynomial fit to a climatology of coldest-0.17%–precipitation rate points around the globe. In each grid box a constant is added to the climatological curve to make it piecewise continuous with the grid box's T_b-precipitation rate curve at the 0.17% T_b. The HQ-IR calibration coefficients computed for a month are applied to each 3-hourly IR data set during that month.

3.3   Merged microwave and IR estimates

It is somewhat challenging to combine the HQ and IR precipitation estimates at individual times because the quantities being sensed tend to have different fine-scale patterns. Accordingly, we simply use the more physically-based HQ estimates "as is" where available, and fill the remaining grid boxes with HQ-calibrated IR estimates. This scheme provides the "best" local estimate, but the time series of precipitation estimates has heterogeneous statistics, including data boundaries in space and time.

3.4   Rescaling to monthly data

The final step in creating the research product is to introduce monthly rain gauge data. Huffman et al. (1997), among others, have demonstrated the advantages of including rain gauge data in combination data sets at the monthly scale, but we were skeptical of including sub-monthly data due to issues of data coverage and timeliness. Rather, we adopt the approach we took in the GPCP One-Degree Daily combination data set, which is to scale the short-period estimates to sum to a monthly estimate that includes monthly gauge data (Huffman et al. 2001). All available 3-hourly merged HQ-IR estimates are summed over the calendar month to create a monthly multi-satellite (MS) product. The MS and gauge are combined using inverse-error-variance weighting as in Huffman et al. (1997) to create a post-real-time monthly satellite-gauge

combination (SG), which is posted by PPS as a separate TRMM product (3B43). Then for each gridbox the (monthly) SG/MS ratio is computed, then applied to scale each 3-hourly field in the month, producing the Version 6 3B42 product. The final fields have the detail of the satellite data, but have nearly neutral monthly bias compared to gauges (i.e., over land).

The output of the 3-hourly algorithm is best viewed as movie loops, examples of which are posted at http://trmm.gsfc.nasa.gov under the button labeled "Realtime 3 Hourly & 7 Day Rainfall".

3.5   RT algorithm adjustments

The RT and research product systems are designed to be as similar as possible to ensure consistency between the resulting data sets. One important difference is that the research product's calibrator, the TCI, is not available in real time. In its absence we use the TMI estimates as the RT calibrator. A second important difference is that a real-time system cannot reach into the future, so the microwave-IR calibration "month" is taken as the five trailing and one current (partial) pentads, or 5-day calendar intervals, of accumulated coincident data. As in the research product, the inter-calibration of individual microwave estimates to the TMI is handled with climatological coefficients. The HQ-IR calibration is recomputed for each 3-hr period to capture rapid changes in the calibration for rare heavy rain events. Third, the monthly gauge adjustment step carried out for the research product is not possible for the RT.

Starting 20 January 2009, we implemented a procedure to address the second and third differences listed above. Preliminary testing showed that computing these adjustments on a climatological basis provoked fewer artifacts than attempting to use data from trailing months. Therefore, we first determine a matched histogram calibration of TMI to the TCI, computed for 10 years of coincident data to establish the climatology for each calendar month. Second, a climatological monthly calibration of TCI to the 3B43 research product is computed as a simple ratio, again on a 1°x1° spatial grid and using 10 years of data. Finally, the TMI-TCI and TCI-3B43 calibrations are successively applied to the preliminary 3-hr RT multi-satellite product to create the final 3B42RT.

4. Current status on Algorithm Development

The research product system is currently running as the Version 6 algorithm for TRMM product 3B-42, although that product provides only the final gauge-adjusted merged microwave-IR field. The Version 6 TRMM 3B-43 product provides the post-real-time monthly SG described above. Version 6 data are available for January 1998 to the (delayed) present at http://lake.nascom.nasa.gov/data/dataset/TRMM/. Users should be aware that beta testing is underway at press time for Version 7, as discussed in Section 6.

The RT system has been running routinely on a best-effort basis in the PPS (originally TSDIS) since late January 2002, and is currently on its sixth release. For simplicity, a fixed latency (currently 9 hours after nominal observation time) triggers the processing. The combined microwave, microwave-calibrated IR, and merged microwave-IR estimates, which are labeled 3B-40RT, 3B-41RT, and 3B-42RT, respectively, are available from ftp://trmmopen.gsfc.nasa.gov or http://precip.gsfc.nasa.gov. All RT estimates created before 7 February 2005 are considered obsolete because they have rather different processing, and therefore should not be used. As part of the release of 20 January 2009 the format for 3B42RT was augmented so that the "new" climatologically-calibrated precipitation estimate is provided in the first ("precip") field, but an

in the first ("precip") field, but an additional field is appended to each file providing the "old" uncalibrated precipitation estimate. This configuration permits users to continue using their previously established analysis routines by accessing the additional precipitation field at the end of each file.

Both data sets (and other precipitation data) are also accessible in the interactive Web-based TRMM On-line Visualizations and Analysis System (TOVAS) at http://lake.nascom.nasa.gov/Giovanni/tovas. The TOVAS site can be particularly helpful for new users, since it allows them to quickly create graphics from any of the TMPA data sets. These results can be used as the standard to validate the data access/navigation/scaling carried out in the users' own application code.

5. Comparisons and Examples

Both versions of the TMPA have been produced for a sufficiently long time that researchers have had the chance to develop and start reporting various applications and validations that employ one or both versions. As well, the TMPA is examined in other chapters in this book <cite specific chapters?>. This section summarizes some of the previous results and provides some test results illustrating the new climatological calibration that was recently instituted in the real-time product.

5.1   Prior results

Basic validation statistics have been reported for a number of locations, including primarily ocean locations (Huffman et al. 2007; Sapiano and Arkin 2008) and primarily land areas (Ebert et al. 2007, among others). The latter set are most interesting to hydrologists, and are notable for the on-going systematic daily continental-scale validation of many different quasi-operational precipitation estimates for Australia, the continental United States, western Europe, parts of South America, and other sites, organized through the the International Precipitation Working Group (IPWG) of the Coordinating Group for Meteorological Satellites (Ebert et al. 2007). The various Web sites for these regions are accessible through http://www.bom.gov.au/bmrc/SatRainVal/validation-intercomparison.html, and each provides a variety of detailed and summary statistics.

The first major result arises from the fact that the histogram of precipitation rates in the microwave input data is generally more accurate over ocean than over land as discussed above. As such, the land estimates are best in convective regimes, where the icy hydrometeors that cause scattering are well-correlated to surface rainfall. It is also the case that the more-approximate IR estimates are better correlated to short-interval precipitation in convective conditions. Conversely, the stratiform clouds that tend to dominate in cool-season and frontal conditions lead to significant mis-estimation using IR algorithms. The behavior for numerical models tend to be the opposite, estimating precipitation more accurately when the model convective parameterizations are not a major factor. As a result, observational estimates, including the TMPA, tend to out-perform models in warm/convective conditions and vice-versa in cool-season stratiform conditions (Ebert et al. 2007).

A second major result is that fine-scale precipitation estimates tend to have high uncertainty, while averaging in space and time improves the error characteristics. As discussed in Huffman et al. (2007), the fine-scale uncertainty arises from a number of issues, including algorithmic uncertainty and variations in the observational characteristics of the various input sensors. Fig. 4 in Huffman et al. (2007) exemplifies the variations among near-simultaneous estimates from

different sensors. Hossain and Huffman (2008), among others, show the systematic improvement in uncertainty that occurs across a number of metrics when increasingly more time/space averaging is applied. The issue, of course, is that many users' applications require the full resolution. Nonetheless, the implicit averaging that results from, say, computing hydrologic drainage basin flows, can allow the relatively uncertain estimates to be useful (Nijssen and Lettenmaier 2004; Hong et al. 2006).

A third major result from previous studies is that the use of monthly gauge analysis data in the post-real-time research TMPA is beneficial, as demonstrated by comparison to the real-time TMPA, which lacks gauge input. This is true at monthly and longer time scales, as one might expect by construction, but it is true even on relatively short intervals (Ebert et al. 2007). This result is the basis for the shift of the real-time TMPA to use of calibration to the post-real-time research TMPA.

A few studies have examined how the histogram of precipitation values compares for the two TMPA products (and other combination algorithms). Typically, the TMPA shows somewhat too many high-precipitation-rate values and lacks precipitation events at the low rates (Fisher and Wolff 2008). The result is that rain areas tend to be too small in size and have conditional rates that are too high. These results are consistent with the finding in Jiang et al. (2008) that the fraction of precipitation produced by tropical cyclones is as much as 30-50% higher in the TMPA than in comparable radar and raingauge data. That is, regions that possess a concentration of high precipitation rates will likely have an excess in the TMPA due to the characteristic bias in the TMPA histograms.

More qualitatively, it is clear that the performance of the TMPA and other combination products is critically dependent on the quality of the input data sets. All of the combination schemes attempt to limit the impact of defects and disparities in the input precipitation data, but the options are limited. For example, the TMPA process starts by auditing the input microwave estimates for possible artifacts based on "ambiguous pixel" flags contained in the GPROF datasets. All microwave datasets are then intercalibrated to a single reference, which is the GPROF-TMI for the real-time product and the TCI (Haddad 1997a,b) for the non-real-time research product. Likewise, the IR calibration is computed from the combined microwave product. These actions should minimize shifts in bias as various satellites contribute intermittently during the day. Issues that cannot be addressed with current tools include: orographic enhancement and warm rain processes in general over land, where only the solid-hydrometeor-based scattering signal is useful; lack of sensitivity to light or very small-scale precipitation; and lack of retrieval skill in frozen surface areas. The older versions of GPROF currently used in the TMPA (and other combinations) display artifacts in some coastal regions, including around inland water bodies (Tian and Peters-Lidard 2007), but it is possible that newer versions of GPROF will correct this issue (Kummerow, personal communication, 2008). There are deficiencies in the current gauge analysis in regions of complex terrain, usually underestimates, but the new analysis available from the GPCC (Schneider et al. 2008) should improve this situation. It will continue to be the case that some underdeveloped areas, such as central Africa, are highly deficient in gauge observations, leading to more uncertainty in those regions for the post-real-time research TMPA.

Additional studies of TMPA performance may be found listed in the document posted at ftp://precip.gsfc.nasa.gov/pub/trmmdocs/TMPA_citations.pdf.

5.2   *Climatological calibration of the RT*

As noted above, the real-time TMPA was upgraded in early 2009 to include a climatological calibration to the post-real-time research TMPA product. Here, we summarize the test data that were used to validate improved performance. Months representative of each season, namely January, April, July, and October in 2007, were computed and then compared to the original uncalibrated RT product. As well, new calibrated RT estimates were computed for October 2008 and similarly examined. The months in 2007 are not fully independent of the calibration coefficients, since 2007 is one of the ten years used in the calibration, but we believe this should not be a critical factor.

The monthly accumulations of all matched 3-hourly estimates for July 2007 from each scheme (Fig. 2) have a very similar visual appearance, but there are important differences (Fig. 3[top], 3[middle]). The Version 6 product is taken as the standard in this discussion, since the reason for the calibration is to make the RT as consistent with Version 6 as possible. The excess precipitation displayed by the original RT (Fig. 3[top]) in Africa, the U.S., and Mesoamerica for this particular month is consistent with typical warm-season results, as are the low values in northeastern Equatorial South America, the Western Ghats in India, and the monsoonal maximum in Bangladesh and surrounding areas. We examine the success of the calibration by defining the improvement (I_{cal}) as

$$I_{cal} = |\ 3B42RT(cal) - 3B42V6\ |\ -\ |\ 3B42RT(uncal) - 3B42V6\ | \tag{1}$$

where each term represents the monthly average of the product named. The calibrated RT is closer to Version 6 in regions where $I_{cal}<0$, while the uncalibrated RT is closer for $I_{cal}>0$. This metric tends to emphasize regions with high precipitation, since a larger dynamic range is possible, but this seems appropriate from a global water and energy balance perspective.

The I_{cal} for July 2007 (Fig. 3[bottom]) demonstrates that most of the regions with biases likely dominated by regimes noted above see improvement with the new calibration scheme (green and blue colors). By comparison with the individual difference images in Figs. 3[top], 3[middle], it is clear that the improvement is frequently in the sense of simply reducing the bias, rather than fully correcting it. The climatological relationships are not always effective for an individual month. Most notably along the coast of Myanmar, but also in the Sahel, western coastal India, southern Japan, and southern Brazil, the calibration drives the result further from correspondence to 3B42V6 for this particular month. We should expect such fluctuations to occur when the selection of regimes experienced in individual months do not match up with the climatological distribution of regimes by month, but future work will include an analysis of such cases for possible design issues with the calibration scheme.

Bias and root-mean-square (RMS) differences are summarized in Table 1 for all, ocean, and land areas in the latitude band 50°N-50°S for July 2007. The bias improves slightly over ocean and degrades slightly over land. These changes are not considered important, since improvements predominantly in regions of one sign could easily drive the latitude-band-average result. The RMS is a more sensitive measure, since it quantifies the degree to which the RT is close to the V6. Improvement in both land and ocean confirms our qualitative impression from Fig. 3 that the calibration is working as intended. The other test months (not shown) tend to show latitude-band-average biases that are only slightly different between the uncalibrated and calibrated RT. The other months' RMS values over land show overall improvement except for January 2007, perhaps because the results are sensitive to the treatment of possible artifacts in cold land conditions.

6. Future Plans/Conclusions

The TMPA is intended to provide a "best" estimate of quasi-global precipitation from the wide variety of modern satellite-borne precipitation-related sensors. Estimates are provided at relatively fine scales (0.25°x0.25°, 3-hourly) in both real and post-real time to accommodate a wide range of research applications. However, the errors inherent in the finest scale estimates are large. The most successful use of the TMPA data takes advantage of the fine-scale data to create averages appropriate to the user's application.

At press time an upgrade of the research quality post-real-time TMPA from Version 6 to Version 7 was in beta test, providing a variety of improvements that modernize the input data sets and correct several issues. Specifically, the latest GPROF code is introduced for SSM/I (including a correction for the channel interference on F15), SSMIS (thus bringing in the F16 and F17 records), AMSR-E, and TMI; improved AMSU-B estimates are used; and MHS estimates from NOAA-18 and MetOp-A are included. The GPCC's improved raingauge analyses are included for both retrospective and initial (i.e., new-data) processing. Finally, we have substantially augmented the data file contents. In 3B42, we are adding fields of merged microwave precipitation, microwave-calibrated IR precipitation, and microwave overpass time, in addition to providing more detail as to the particular sensor on which the final precipitation estimate is based. In 3B43 we are including a data field for the relative weighting that the gauges receive in each grid box.

The immediate task at hand is to complete the current beta test of the Version 7 TMPA system, reprocess the TRMM archive, and commence Version 7 computations on new observations. Once Version 7 is established, presumably in late 2009, Version 6 will be considered obsolete. As well, at that point the climatological calibrations in the RT will be updated to Version 7, rendering the Version 6-calibrated RT obsolete. Status messages are posted routinely in the "Information" hot link buttons on http://precip.gsfc.nasa.gov for the respective products.

Looking to the future, we are studying how best to extend the TMPA to higher latitudes, for example by incorporating fully global precipitation estimates based on Television Infrared Observation Satellite (TIROS) Operational Vertical Sounder (TOVS), Advanced TOVS (ATOVS), and Advanced Infrared Sounder (AIRS) data. It is also a matter of research to work toward a Lagrangian time interpolation scheme, conceptually along the lines of the CPC Morphing (CMORPH) algorithm (Joyce et al. 2004) and the Global Satellite Map of Precipitation (GSMaP; Kubota et al. 2007). Finally, it is still the case that the study of precipitation in general needs a succinct statistical description of how errors in fine-scale precipitation estimates should be aggregated through scales up to global/monthly (Hossain and Huffman 2008).

On the instrumentation side there is a concerted effort to provide complete 3-hourly microwave data. Most of this effort is focused on the National Aeronautics and Space Administration's Global Precipitation Measurement (GPM) project. Besides simply increasing the frequency of coverage, it is planned for GPM to provide a TRMM-like "core" satellite to calibrate all of the microwave estimates on an on-going basis. We expect the geo-IR–based estimates to have a long-term role in filling the inevitable gaps in microwave coverage, as well as in enabling sub-3-hourly precipitation estimates at fine spatial scales.

References

Adler RF, Huffman GJ, Chang A, Ferraro R, Xie P, Janowiak JE, Rudolf B, Schneider U, Curtis S, Bolvin DT, Gruber A, Susskind J, Arkin PA, Nelkin EJ (2003) The Version 2 Global Precipitation Climatology Project (GPCP) monthly precipitation analysis (1979-present). *J. Hydrometeor.* **4**:1147-1167

Adler RF, Huffman GJ, Keehn PR (1994) Global tropical rain estimates from microwave-adjusted geosynchronous IR data. *Remote Sensing Rev.* **11**:125-152

Arkin PA, Meisner BN (1987) The relationship between large-scale convective rainfall and cold cloud over the Western Hemisphere during 1982-1984. *Mon. Wea. Rev.* **115**:51-74

Ebert EE, Janowiak JE, Kidd C (2007) Comparison of near real time precipitation estimates from satellite observations and numerical models. *Bull. Amer. Meteor. Soc.* **88**:47-64

Fisher BL, Wolff DB (2008) Validating microwave-based satellite rain Rate retrievals over TRMM Ground Validation sites. Amer. Geophys. Union (AGU) Fall Meeting, 15-19 December 2008, San Francisco, CA

Haddad ZS, Smith EA, Kummerow CD, Iguchi T, Farrar MR, Durden SL, Alves M, Olson WS (1997a) The TRMM "Day-1" radar/radiometer combined rain-profiling algorithm. *J. Meteor. Soc. Japan* **75**,:799-809

Haddad ZS, Short DA, Durden SL, Im E, Hensley S, Grable MB, Black RA (1997b) A new parameterization of the rain drop size distribution. *IEEE Trans. Geosci. Rem. Sens.* **35**:532-539

Hong Y, Adler R, Hossain F, Curtis S (2007) Global runoff simulation using satellite rainfall estimation and SCS-CN method. *Water Resources Res* 43(W08502) doi:10.1029/2006WR005739

Hossain F, Huffman GJ (2008) Investigating error metrics for satellite rainfall data at hydrologically relevant scales. *J. Hydrometeor.* **9**:563-575

Huffman GJ, Adler RF, Arkin P, Chang A, Ferraro R, Gruber A, Janowiak J, McNab A, Rudolf B, Schneider U (1997) The Global Precipitation Climatology Project (GPCP) combined precipitation data set. *Bull. Amer. Meteor. Soc.* **78**:5-20

Huffman GJ, Adler RF, Bolvin DT, Gu G, Nelkin EJ, Bowman KP, Hong Y, Stocker EF, Wolff DB (2007) The TRMM Multi-satellite Precipitation Analysis: Quasi-global, multi-year, combined-sensor precipitation estimates at fine scale. *J. Hydrometeor.* **8**:38-55

Huffman GJ, Adler RF, Morrissey M, Bolvin DT, Curtis S, Joyce R, McGavock B, Susskind J (2001) Global precipitation at one-degree daily resolution from multi-satellite observations. *J. Hydrometeor.* **2**:36-50

Janowiak JE, Joyce RJ, Yarosh Y (2001) A real-time global half-hourly pixel-resolution IR dataset and its applications. *Bull. Amer. Meteor. Soc.* **82**:205-217

Jiang H, Halverson JB, Simpson J (2008) On the differences in storm rainfall from Hurricanes Isidore and Lili. Part I: Satellite observations and rain potential. *Wea. Forecasting* **23**:44–61

Joyce RJ, Janowiak JE, Arkin PA, Xie P (2004) CMORPH: A method that produces global precipitation estimates from passive microwave and infrared data at high spatial and temporal resolution. *J. Hydrometeor.* **5**:487–503

Krajewski WF, Smith JA (1991) On the estimation of climatological Z–R relationships. *J. Appl. Meteor.* **30**:1436–1445

Kubota T, Shige S, Hashizume H, Aonashi K, Takahashi N, Seto S, Hirose M, Takayabu YN, Nakagawa K, Iwanami K, Ushio T, Kachi M, Okamoto K (2007) Global precipitation map

using satellite-borne microwave radiometers by the GSMaP Project: Production and validation. *IEEE Trans. Geosci. Remote Sens*. **45**:2259-2275

Kummerow, C., W.S. Olson, L. Giglio, 1996: A simplified scheme for obtaining precipitation and vertical hydrometeor profiles from passive microwave sensors. *IEEE Trans. Geosci. Remote Sens.* **34**:1213-1232

Miller JR (1972) A climatological Z-R relationship for convective storms in the northern Great Plains. *15th Conf. on Radar Meteor.* 153-154

Nijssen B, Lettenmaier DP (2004) Effect of precipitation sampling error on simulated hydrological fluxes and states: Anticipating the Global Precipitation Measurement satellites. *J. Geophys. Res.* 109(D02103)

Olson WS, Kummerow CD, Hong Y, Tao W-K (1999) Atmospheric latent heating distributions in the Tropics derived from satellite passive microwave radiometer measurements. *J. Appl. Meteor.*, **38**:633–664

Rudolf B (1993) Management and analysis of precipitation data on a routine basis. *Proc. Internat. Symp. on Precip. and Evap.* (Eds. B. Sevruk, M. Lapin), 20-24 Sept. 1993, Slovak Hydrometeor. Inst., Bratislava, Slovak Rep. **1**:69-76

Sapiano MRP, Arkin PA (2008) An inter-comparison and validation of high resolution satellite precipitation estimates with three-hourly gauge data. *J. Hydrometeor.* in press

Schneider U, Fuchs T, Meyer-Christoffer A, Rudolf B (2008) Global precipitation analysis products. File GPCC_intro_products_2008.pdf at http://gpcc.dwd.de/. Accessed 8 December 2008

Tian Y, Peters-Lidard CD (2007) Systematic anomalies over inland water bodies in satellite-based precipitation estimates. *Geophys. Res. Lett.* **34**(L14403)

Xie P, Arkin PA (1996) Gauge-based monthly analysis of global land precipitation from 1971 to 1994. *J. Geophys. Res.* **101**:19023-19034

Weng F, Zhao L, Ferraro R, Poe G, Li X, Grody N (2003) Advanced Microwave Sounding Unit cloud and precipitation algorithms. *Radio Sci.* **38**:8068–8079

Zhao L, Weng F (2002) Retrieval of ice cloud parameters using the Advanced Microwave Sounding Unit. *J. Appl. Meteor.*, **41**:384-395

Table Legends

1. Bias and root-mean–square (RMS) difference statistics comparing monthly accumulations of uncalibrated and calibrated 3B42RT estimates, compared to the Version 6 3B42. Results are displayed for all, ocean, and land regions in the latitude band 50°N-50°S for July 2007 in units of mm/d.

Figure Captions

1. Time history of Equator-crossing times (in Local Standard Time) of precipitation-sensing microwave satellites/sensors through September 2008. All are ascending node, except for DMSP F08 and MetOp-A. The thickest lines denote the satellite used as a calibrator in the GPCP datasets. TRMM is denoted by shading because it precesses, covering all overpass times in the course of a 43-day period.
2. Average precipitation rate in mm/d for July 2007 for the (top) uncalibrated RT, (middle) calibrated RT, and (bottom) V6 TMPA precipitation products.
3. Monthly average difference between (top) uncalibrated RT and V6, and (middle) calibrated RT and V6. (bottom) Improvement metric defined in Eq. 1, I_{cal}, which is the absolute value of the top image subtracted from the absolute value of the middle image. In all three panels the units are mm/d, the data are for July 2007, and the fields referenced are displayed in Fig. 2.

Table 1. Bias and root-mean–square (RMS) difference statistics comparing monthly accumulations of uncalibrated and calibrated 3B42RT estimates, compared to the Version 6 3B42. Results are displayed for all, ocean, and land regions in the latitude band 50°N-50°S for July 2007 in units of mm/d.

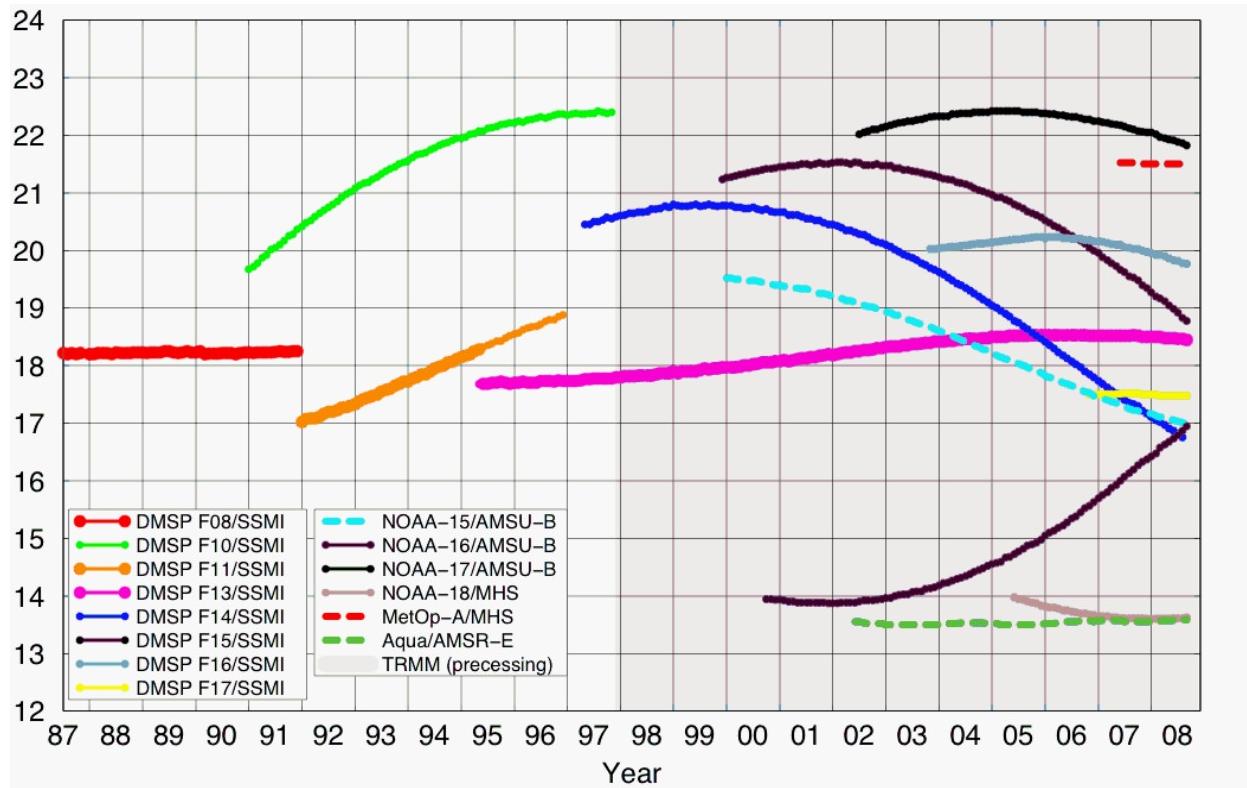| Region	RT(uncal)–V6 bias (mm/d)	RT(cal)–V6 bias (m/d)	RT(uncal)–V6 RMS (mm/d)	RT(cal)–V6 RMS (mm/d)
All	0.048	0.181	1.49	1.23
Ocean	-0.079	0.053	1.04	0.95
Land	0.399	0.535	2.31	1.78

Fig. 1 Time history of Equator-crossing times (in Local Standard Time) of precipitation-sensing microwave satellites/sensors through September 2008. All are ascending node, except for DMSP F08 and MetOp-A. The thickest lines denote the satellite used as a calibrator in the GPCP datasets.   TRMM is denoted by shading because it precesses, covering all overpass times in the course of a 43-day period.
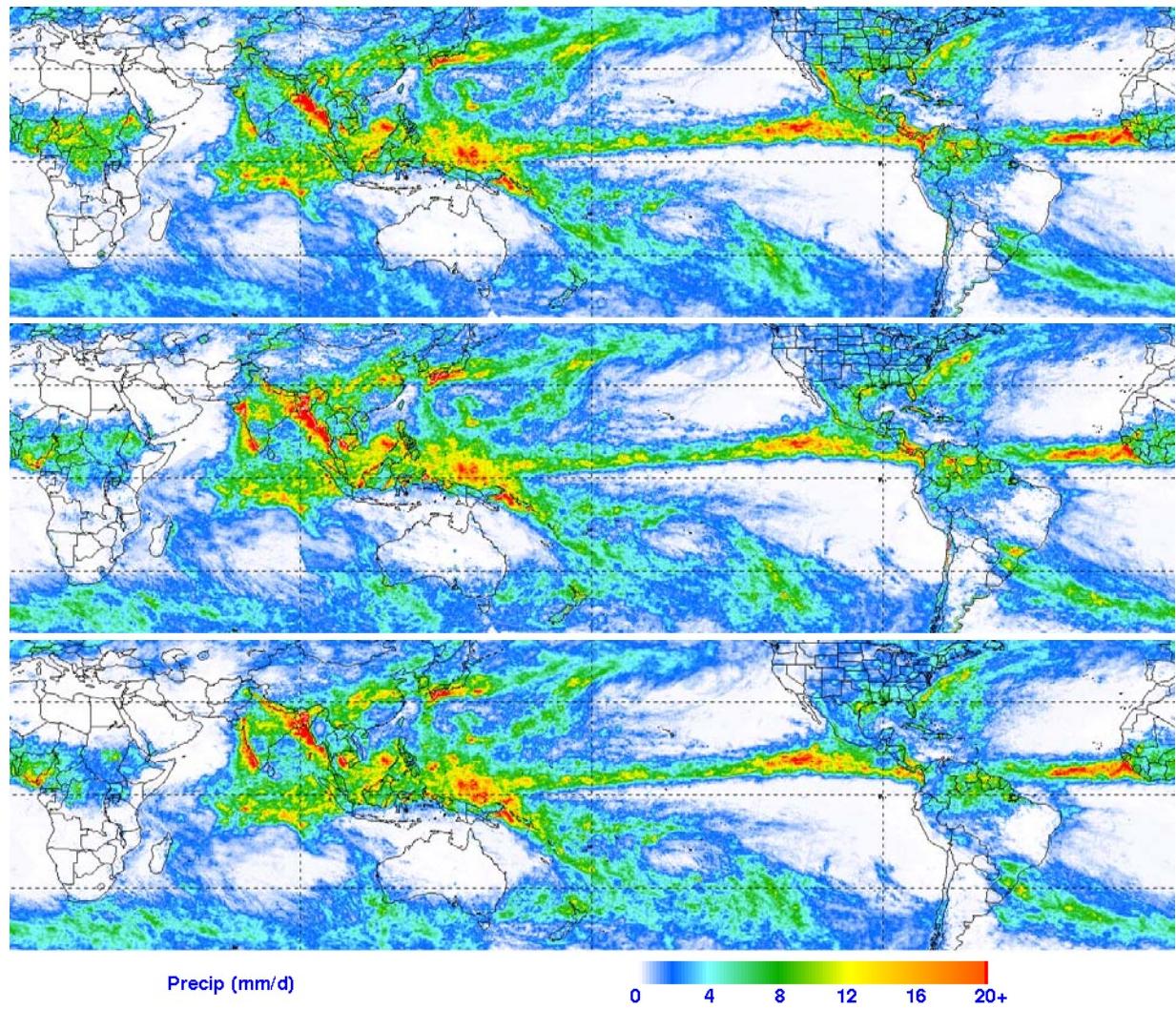
Fig. 2 Average precipitation rate in mm/d for July 2007 for the (top) uncalibrated RT, (middle) calibrated RT, and (bottom) V6 TMPA precipitation products.

Precip Difference (mm/d)

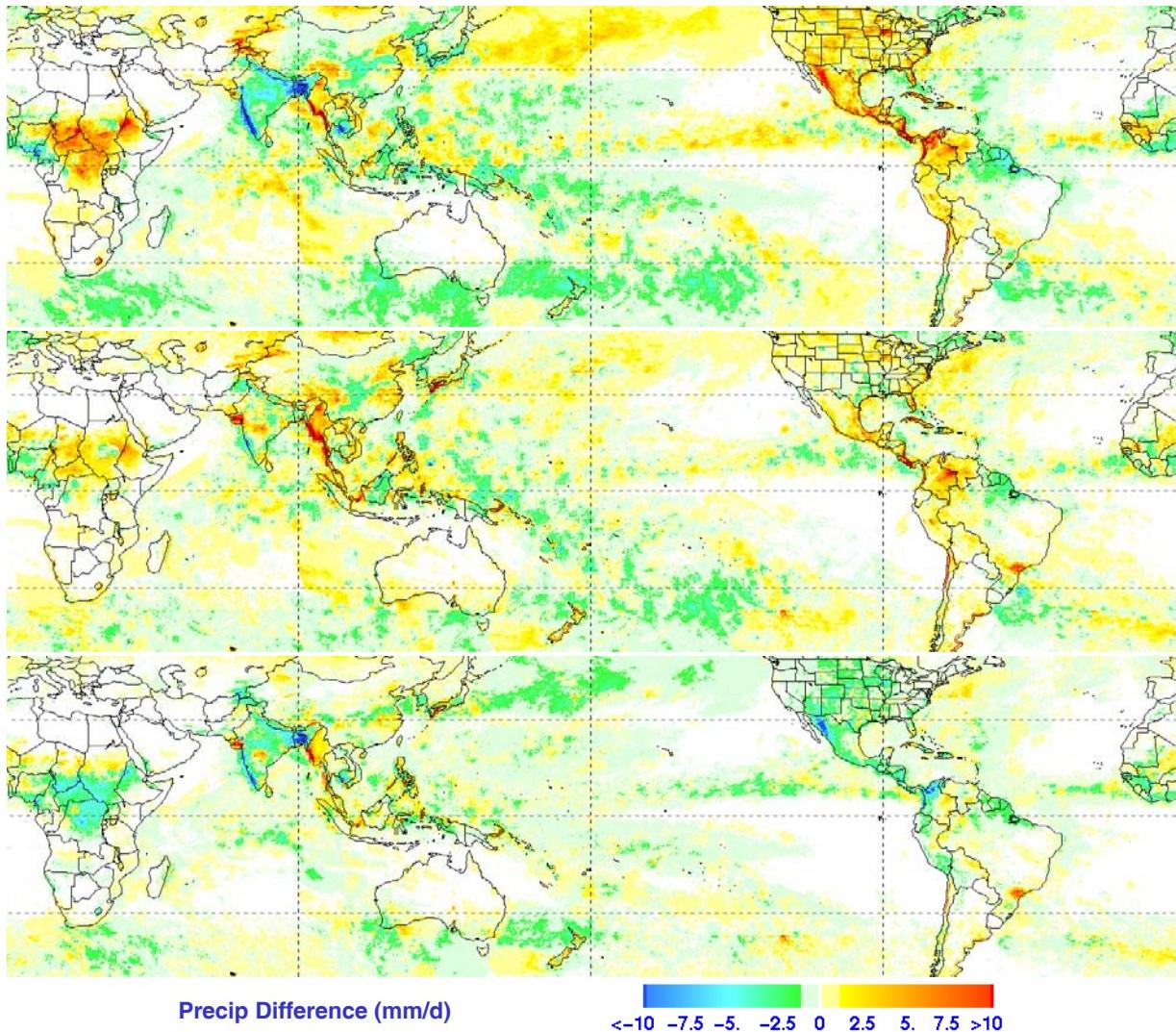<-10 -7.5 $-5.$ -2.5 0 2.5 $5.$ 7.5 >10

Fig. 3 Monthly average difference between (top) uncalibrated RT and V6, and (middle) calibrated RT and V6. (bottom) Improvement metric defined in Eq. 1, I_{cal}, which is the absolute value of the top image subtracted from the absolute value of the middle image. In all three panels the units are mm/d, the data are for July 2007, and the fields referenced are displayed in Fig. 2.